Interplay of interfacial layers and blend composition to reduce thermal degradation of polymer solar cells at high temperature

ACS APPLIED MATERIALS & INTERFACES

Article

Interplay of interfacial layers and blend composition to reduce thermal degradation of polymer solar cells at high temperature

Sadok Ben Dkhil, Martin Pfannmöller, Rasmus R. Schroeder, Riva Alkarsifi, Meriem Gaceur, Wolfgang Köntges, Hamed Heidari, Sara Bals, Olivier Margeat, Jörg Ackermann, and Christine Videlot-Ackermann

ACS Appl. Mater. Interfaces, **Just Accepted Manuscript** • DOI: 10.1021/acsami.7b17021 • Publication Date (Web): 12 Jan 2018

Just Accepted

ACS Publications

ACS Applied Materials & Interfaces is published by the American Chemical Society.
1155 Sixteenth Street N.W., Washington, DC 20036

Interplay of interfacial layers and blend composition to reduce thermal degradation of polymer solar cells at high temperature

Sadok Ben Dkhil,[1] Martin Pfannmöller,[2,#] Rasmus R. Schröder,[3] Riva Alkarsifi,[1] Meriem Gaceur,[1] Wolfgang Köntges,[3] Hamed Heidari,[2] Sara Bals,[2] Olivier Margeat,[1] Jörg Ackermann,[1,] Christine Videlot-Ackermann.[1,]**

[1] Aix Marseille Univ., UMR CNRS 7325, CINaM, Marseille, France.

[2] University of Antwerp, Electron Microscopy for Materials Research (EMAT), Groenenborgerlaan 171, 2020 Antwerp, Belgium.

[3] Centre for Advanced Materials, Heidelberg University, 69120 Heidelberg, Germany.

* Corresponding authors: ackermann@cinam.univ-mrs.fr; videlot@cinam.univ-mrs.fr

[#] Present address: Centre for Advanced Materials, Heidelberg University, 69120 Heidelberg, Germany

Abstract

The thermal stability of printed polymer solar cells at elevated temperatures needs to be improved to achieve high-throughput fabrication including annealing steps as well as long-term stability. During device processing, thermal annealing impact both the organic photoactive layer and the two interfacial layers making detailed studies of degradation mechanism delicate. A recently identified thermally stable PTB7:$PC_{70}BM$ blend as photoactive layer in combination with PEDOT:PSS as hole extraction layer is used here to focus on the impact of electron extraction layer (EEL) on the thermal stability of solar cells. Solar cells processed with densely packed ZnO nanoparticle layers show still 92% of the initial efficiency after constant annealing during one day at 140°C, while partially covering ZnO layers as well as an evaporated calcium layer lead to performance losses up to 30%. This demonstrates that the nature and morphology of EELs highly influence the thermal stability of the device. We extend our study to thermally unstable PTB7:$PC_{60}BM$ blends to highlight the impact of ZnO on the device degradation during annealing. Importantly, only 12% loss in photocurrent density is observed after annealing at 140°C during one day when using closely packed ZnO. This is in stark contrast to literature and addressed here to the use of a stable double-sided confinement during thermal annealing. The underlying mechanism of the inhibition of photocurrent losses is revealed by electron microscopic imaging and spatially resolved spectroscopy. We found that the double-sided confinement suppresses extensive fullerene diffusion during annealing step, but with still an increase in size and distance of the enriched donor and acceptor domains inside the photoactive layer by an average factor of five. The later result in combination with comparably small photocurrent density losses indicates the existence of efficient transport of minority charge carriers inside donor and acceptor enriched phases in PTB7:$PC_{60}BM$ blends.

Keywords: Polymer solar cells, interfacial layer, ZnO nanoparticles, nanoscale morphology, thermal stability.

1. Introduction

In the competitive field of renewable energy sources, polymer solar cells (PSCs) are nowadays promising candidates for niche markets. Thanks to extensive research in novel organic semiconductors and device structures, PSCs have reached power conversion efficiencies (PCEs) over 13% at lab scale level and 7% at module level.[1-8] However, efficiency and stability of PSCs using high-throughput roll-to-roll (R2R) processing are still low hindering limiting their introduction into the market. PSCs are multi-layer devices that require successive annealing steps up to 140°C during processing of each layer.[9] Therefore, thermal stability of each material used in PSC processing remains one of the most challenging factors, especially as a temperature increase occurs not only during processing but also inevitably during operation under illumination. Thermal stability is also a key challenge for other solution processed photovoltaic technologies such as efficiency perovskite solar cells involving constant efforts to enhance the device stability and durability.[10-13] Since PSCs are formed of stacked layers, performance losses can be related to degradation of electronic properties in each layer constituting the device, i.e. electrodes, interfacial layers (ILs) and photoactive layer.[9,14-17] The photoactive layer of high efficiency organic devices consists of a bulk heterojunction (BHJ) that is a bicontinuous interpenetrating network of nano-sized donor- and acceptor-enriched phases. By the fact that the BHJ is generally a meta-stable state, thermal stress will introduce phase separation leading to micrometer-sized domains of acceptor molecules inside the polymer blend and thus a loss in photocurrent. In the case of fullerene acceptors, their diffusion through the polymer donor phase leads to the formation of large fullerene crystals via Ostwald ripening, which is considered to be the main factor for thermal instability.[9,14,15,18]

Over the last decade thermal stability of PSCs related to the photoactive layer has be studied intensively and was improved by a large palette of approaches.[19-38] However, the impact of the interfacial buffer layers—which are highly relevant for the performance of the solar cells—on the thermal stability of the solar cells has only be considered marginally.[39,40] For example, it is known that metal ions can diffuse into the organic layer creating substantial leakage current.[41,42] Furthermore, chemical reactions at the metal/organic interface can alter the contact properties, forming interfacial dipole barriers and defect states that pin the Fermi level.[43,44] It is important to mention that investigation of the thermal degradation of PSCs related to the ILs is very delicate because thermal annealing can also degrade the BHJ simultaneously. Due to this strong interplay between photoactive layer and ILs, the stability of the photoactive layer is typically studied by thermal annealing of the polymer blend followed by successive deposition of the IL and the electrode to complete the device. By consequence, the photoactive layer is therefore often annealed in the condition of single-sided confinement. Recently, we have demonstrated that high efficiency solar cells with unprecedented thermal stability at 140°C over several days can be obtained when using a double-sided or sandwich-like confinement during thermal annealing, defined as a post-annealing in the following.[38,45] We used a regular device structure composed of solution processed ILs with hole extraction layers (HELs) based on poly(3,4-ethylenedioxythiophene) polystyrene sulfonate polymer (PEDOT:PSS) and electron extraction layers (EELs) made of ZnO nanoparticles; the devices were completed by evaporated Al cathodes.[38] The photoactive layer consisted of a low band gap polymer poly[[4,8-bis[(2-ethylhexyl)oxy]benzo[1,2-b:4,5-b']dithiophene-2,6-diyl][3-fluoro-2-[(2-ethylhexyl)carbonyl]thieno[3,4-b]thiophenediyl]] (PTB7) blended with [6,6]-Phenyl-C71-butyric acid methyl ester ($PC_{70}BM$). We could show that fullerene diffusion was suppressed in PTB7:$PC_{70}BM$ blends while annealing at 140°C. The thermal stability of the blend was attributed to highly stable mixed phases, forming PTB7:$PC_{70}BM$ aggregates and inhibiting fullerene diffusion between polymer- and fullerene-enriched phases. It is important

to highlight that those results also suggest that the used ILs, namely PEDOT:PSS and ZnO, were thermally stable.

Here, we study more in details the degradation mechanisms in PSCs under thermal stress related to cathode buffer material and morphology in combination with PTB7:fullerene blends. Amongst the large choice of EEL materials including organic and inorganic materials,[39,40,46] we selected ZnO and calcium (Ca) as both materials were used in former stability studies of regular device structures using PTB7 donor polymers.[32,38] Furthermore both materials allow EEL processing with varying layer thicknesses and thus morphologies without alternating device performance strongly. By using first PTB7:$PC_{70}BM$ blend as thermally stable active layer we demonstrate that only densely packed ZnO layers generate high thermal stability, while partially covered or porous ZnO layers leads to strong degradation. In contrast that Ca based EELs lead to strong performance losses up to 40% after a constant post-annealing at 140°C independently of layer morphology. These results show the importance of both material selection and layer morphology for EELs to gain thermal stability. Furthermore the thermally stable ILs were used to perform a detailed investigation of the thermal degradation of solar cells using a known thermally unstable polymer blend, namely PTB7 mixed with the smaller fullerene derivative $PC_{60}BM$,[30,32] during annealing in a double-sided confinement. We show that the photocurrent density in PTB7:$PC_{60}BM$ solar cells using the double-sided confinement is only reduced by 12%. This leads to an overall efficiency of 3.2% after a constant post-annealing at 140°C over 1 day, which is in stark contrast to literature where much stronger degradation is observed when using a single-sided confinement.[30,32] The underlying mechanism of the improved thermal stability is addressed to reduced fullerene diffusion on the blend surface using the double-sided confinement, which inhibits the formation of large fullerene crystals on the blend surface. Importantly analytical electron microscopy (electron spectroscopic imaging, ESI) is used for the first time to visualize morphological changes in the PTB7:$PC_{60}BM$ blend under thermal annealing. We could show

that although photocurrent density only drops by 12% there is an increase in size and distance of the enriched donor and acceptor domains by an average factor of 5. The observed photocurrent losses due to the morphological changes are discussed in the context of exciton diffusion and ambipolar transport inside the mixed and the donor-enriched phases, but also in the acceptor-enriched phase.

2. Experimental Section

Materials. ZnO nanocrystals and ZnO-based solutions were prepared as published elsewhere.[47,48] Cluster free ZnO nanocrystal solutions in isopropanol at 7.5 mg/mL were prepared by mixing 0.2 vol.% of ethanolamine (EA). PTB7 was purchased from 1-Materials, $PC_{60}BM$ and $PC_{70}BM$ with a purity of 99 % were purchased from Solemn and Nano-C, respectively. The solvent additive 1,8-diiodoctane (DIO) was purchased from Sigma-Aldrich.

Solar cell fabrication and characterization. Solar cells using PTB7 as donor in regular device structure were processed as detailed in former work.[38] ITO substrates (purchased from Lumtec, 15 $Ohm.sq^{-1}$) were thoroughly cleaned by sonication in acetone and ethanol followed by rinsing with water and sonication in isopropanol. A final ultraviolet-ozone treatment was applied for 15 min. A thin layer of poly(3,4-PEDOT:PSS) (CLEVIOS^{TM} AI 4083) was spin-coated on the cleaned ITO pre-coated glass substrate at the speed of 4000 rpm for 60 s followed by an annealing step on a hot-plate at 140°C for 15 min leading to a layer thickness of 40 nm. The substrates were then transferred to a nitrogen-filled glove box. PTB7 (concentration of 10 $mg.mL^{-1}$) was mixed with $PC_{70}BM$ or $PC_{60}BM$ (ratio of 1:1.5) in solvent mixture of chlorobenzene and 1,8-diiodoctane (DIO) at 97:3% volume ratio. The PTB7:$PC_{70}BM$ and PTB7:$PC_{60}BM$ blends with a nominal thickness of 90 nm were prepared by spin-coating the corresponding solution at 1800 rpm for 2 min. After dried in vacuum overnight, different interfacial layers (ILs) were processed on top of the photoactive layer. ILs based on ZnO nanoparticles were processed by spin-coating ZnO inks, with a concentration of

7.5 mg/mL and 0.2 vol.% of ethanolamine, on top of the active layers at 1500 rpm for 60 s followed by annealing for 5 min at 80°C; all processes were done inside the glovebox. ILs of calcium (Ca) were processed by thermally evaporation at 1×10^{-7} Torr to a thickness of either 10 nm or 30 nm. Aluminum (Al) metal electrodes were thermally evaporated (MBRAUN evaporator) at 2×10^{-6} Torr to a thickness of 100 nm using a shadow mask that define the device area of the solar cells to 0.27 cm^2.

The current density–voltage (J-V) characteristics of the solar cells were measured inside the glove box using a Keithley 238 Source Measure Unit and a Newport class AAA 1.5 Global solar simulator (Oriel Sol3ATM model n° 94043A) with an irradiation intensity of 100 mW/cm^2. The light intensity was determined with a Si reference cell (Newport Company, Oriel n°94043A) calibrated by National Renewable Energy Laboratory (NREL). Spectral mismatch factors (M) were calculated according to a standard procedure and a typical M value of 1.02 was obtained for the PTB7:$PC_{70}BM$ devices.[47] The value was used to correct the measured J_{sc} values of the solar cells to J_{sc} values corresponding to AM1.5G conditions. Shadow masks were used to well-define the illuminated area to 0.27×1.0 cm^2. We present performance of the best devices, while average PCEs were obtained with standard deviation analysis calculated using 9 devices.

External quantum efficiency (EQE) measurements were performed in air using a homemade setup consisting of a Keithley 238 Source Measure Unit and Newport monochromator. Light intensity was measured with a calibrated Si-diode from Newport Company.

Thermal stress application. The thermal stress treatments were applied to stack layers in a double- or single-sided confinement. The thermal annealing at 140°C was either applied directly on the complete PTB7:$PC_{60}BM$ solar cell (defined as the post-annealing) or before the ZnO and Al depositions (defined as the pre-annealing) on a hot plate at 140°C inside the glovebox during a controlled time.

Morphological analysis. The surface morphology of the ZnO layers was studied by atomic force microscopy (AFM) using a Nanoscope III in taping mode. Light microscope analyses were performed with a confocal laser scanning microscope (LSM710 Zeiss) on layers deposited on glass substrate with identical deposition parameters as used in solar cells and exposed to the annealing temperature (140°C) in air. In order to visualize the nanoscale morphology of PTB7:$PC_{60}BM$ blends under double side confinement inside the device, we processed first a layer stack composed of ITO/PEDOT:PSS/PTB7:$PC_{60}BM$/ZnO under identical conditions. After annealing of the whole stack we applied ESI analyses to the samples to visualize the blend morphology via measuring through the ZnO layer. The photoactive layers with and without ZnO were floated on top of deionized water by dissolving the PEDOT:PSS layer. Pieces of the floating layer were collected with a grid covered with holey carbon film (QUANTIFOIL®). For non-annealed sample of PTB7:$PC_{60}BM$ that are not covered with ZnO, ESI measurements were performed in transmission electron microscopy mode with a Libra 200 MC microscope (Carl Zeiss Microscopy, Germany) at 60 kV acceleration voltage using series of energy-filtered images as previously shown.[49] ESI measurements and dark-field images for all other layers were recorded in a Titan 60-300 microscope (Thermo Fisher Scientific, USA). Since some samples were covered with the additional ZnO layer, a larger inelastic mean-free path was achieved by raising the electron energy to 120 keV. Single-scattering distributions were computed by Fourier-log deconvolution allowing unambiguous fitting of the bulk plasmon peak energies. These energies were spatially mapped out in 2D images to represent morphological maps. Layers covered with ZnO were still below a total of 100 nm in thickness, thus layers were thin enough to assume to a first approximation a linear contribution of the different materials to the energy-loss spectra. To determine the ZnO contribution to the spectra, reference spectra of pure materials were measured. The STEM-ESI data sets were then fitted to the three pure spectra as reference data (PTB7, $PC_{60}BM$, and ZnO) by a multiple linear least-squares

algorithm. The contribution of ZnO was subtracted from the measured mixed signal pixel by pixel, i.e. spectrum by spectrum, so that the subsequently determined plasmon peak energy represents the signals from the organic active layer only. All data processing of ESI spectra was performed using HyperSpy (http://hyperspy.org).

3. Results and Discussion

The device and the molecular structures of the donor and acceptor materials are shown in **Figure 1**. PEDOT:PSS was applied as the HEL material at constant thickness, while ZnO and Ca were used as EEL materials, with different layer thickness and morphology to study their impact on the device stability. Devices with bare aluminium (Al) cathode and bare indium tin oxide (ITO) anode were studied as references.

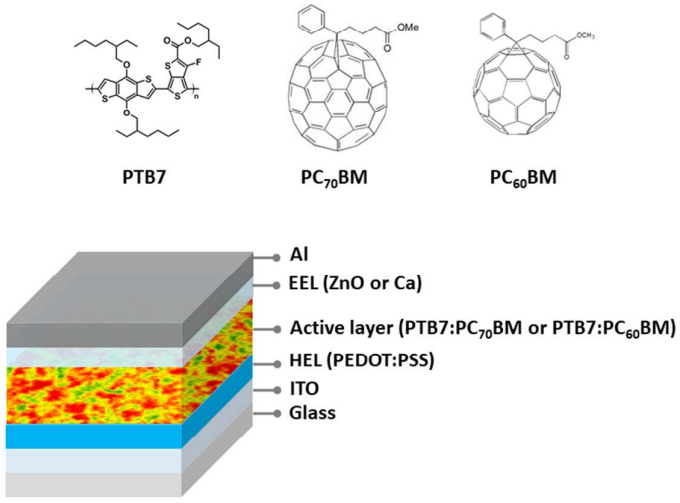

Figure 1. Molecular structures of PTB7, $PC_{70}BM$, and $PC_{60}BM$ together with the schematic multi-layer device structure of solar cells.

3.1 Interfacial layer related thermal degradation of polymer solar cells

To study the role of EELs in detail, we first compare the performances of PTB7:$PC_{70}BM$ solar cells using either ZnO/Al or Ca/Al contacts with devices using bare Al contacts. The

entire devices were exposed to a post-annealing treatment of 140°C of various times. This means that the PTB7:$PC_{70}BM$ blend layers are annealed in a double-sided confinement. **Table 1** and **Figure 2** present the time evolution of photovoltaic parameters (fill factor FF, short-circuit density J_{sc}, open-circuit current $V_{oc,}$ and, power conversion efficiency PCE) for the different devices under a constant thermal stress at 140°C up to 3 days. The corresponding J-V curves are shown in **Figure S1**.

Table 1. Photovoltaic parameters (PCE, V_{oc}, J_{sc} and FF; additionally an average PCE of 9 devices with standard deviation is provided) of PTB7:$PC_{70}BM$ solar cells exposed continuously to a post-annealing thermal stress at 140°C up to 3 days processed with the following device structures:

- ITO/PEDOT:PSS/PTB7:$PC_{70}BM$/**ZnO/Al** with ZnO as interfacial layer
- ITO/PEDOT:PSS/PTB7:$PC_{70}BM$/**Ca/Al** with Ca as interfacial layer
- ITO/PEDOT:PSS/PTB7:$PC_{70}BM$/**Al** with bare Al contact
- **ITO**/PTB7:$PC_{70}BM$/ZnO/Al with bare ITO contact

	PCE (%)	V_{oc} (mV)	J_{sc} (mA/cm^2)	FF (%)	Average PCE (± std. dev.)
ZnO/Al					
As-prepared	8.38	765	15.86	69	8.22 ± 0.11
140°C 10 min	7.8	785	16.08	62	7.52 ± 0.19
140°C 1 hour	7.84	786	16.13	62	7.49 ± 0.23
140°C 1 day	7.79	787	16.18	61	7.58 ± 0.19
140°C 2 days	7.67	788	16.22	60	7.4 ± 0.25
140°C 3 days	7.62	789	16.19	60	7.26 ± 0.22
Ca/Al					
As-prepared	7.60	745	14.62	70	7.49 ± 0.11
140°C 10 min	6.72	789	14.30	60	6.43 ± 0.21
140°C 1 hour	6.49	790	14.06	58	6.24 ± 0.16
140°C 1 day	6.07	785	13.64	57	5.51 ± 0.40
140°C 2 days	5.38	773	13.18	53	4.85 ± 0.49
140°C 3 days	4.40	734	12.92	46	3.64 ± 0.50
bare Al					
As-prepared	5.70	671	15.28	56	5.45 ± 0.20
140°C 10 min	5.46	740	14.10	52	5.27 ± 0.14
140°C 1 hour	5.32	726	14.28	51	5.03 ± 0.27
140°C 1 day	4.01	598	14.20	47	3.46 ± 0.38
140°C 2 days	3.81	595	14.02	46	3.33 ± 0.34
140°C 3 days	3.65	593	13.86	44	2.96 ± 0.58
bare ITO					
As-prepared	2.38	387	14.31	43	2.15 ± 0.21
140°C 10 min	1.69	349	11.29	43	1.36 ± 0.25
140°C 1 hour	0.84	223	9.97	38	0.5 ± 0.26
140°C 3 days	0.42	168	7.51	34	0.22 ± 0.13

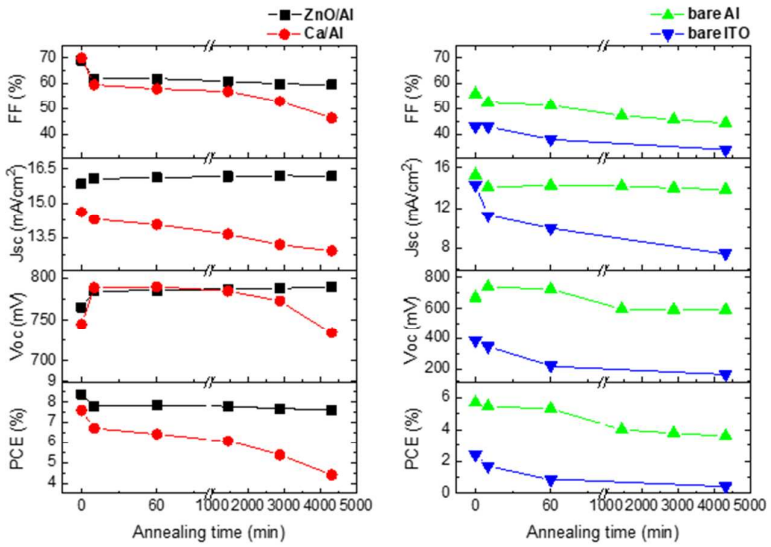

Figure 2. Time evolution of photovoltaic parameters of PTB7:$PC_{70}BM$ solar cells exposed continuously to a post-annealing thermal stress at 140°C up to 3 days processed with the following device structures: ITO/PEDOT:PSS/PTB7:$PC_{70}BM$/ZnO/Al with a ZnO interfacial layer (black squares), ITO/PEDOT:PSS/PTB7:$PC_{70}BM$/Ca/Al with a Ca interfacial layer (red circles), ITO/PEDOT:PSS/PTB7:$PC_{70}BM$/Al with a bare Al contact (green up triangles) and ITO/PTB7:$PC_{70}BM$/ZnO/Al with a bare ITO contact (blue down triangles).

While devices using ZnO/Al contacts are stable over the whole period of observation, solar cells using Ca buffer layers show a continuous degradation of FF, J_{sc} and thus PCE under a thermal stress at 140°C. Only the V_{oc} shows a spontaneous increase under the post-annealing at 140°C in both cases. The later can be addressed to the diffusion of fullerene to the blend surface during the first minutes of annealing induced by the DIO evaporation. The accumulation of fullerene at the blend surface improves then the charge carrier extraction at the cathode and thus Voc.[38] Similar increase in V_{oc} is observed for solar cells using a bare Al contact. The losses of PCE when using Ca are primarily ascribed to strong losses in J_{sc} and FF. This can be attribute to thermally activated Ca ion diffusion and/or chemical reaction of Ca with the polymer blend. Both processes lead to strongly increased recombination.[9] In case of

the bare Al contact, only the FF constantly decreases, which can be addressed to chemical reaction of Al with the polymer surface inducing an increasing amount of recombination centres.[9] Importantly, we show that ZnO is a highly stable EEL material as almost unaltered J-V curves (see **Figure S1**) and photovoltaic parameters (see **Table 1** and **Figure 2**) are observed under post-annealing treatment at 140°C during 3 days. This proves that the electronic properties of ZnO EELs as well as the ZnO/polymer blend interfaces are stable under thermal stress at 140°C. Furthermore, ZnO efficiently protects the polymer blend against thermally induced damages from the Al electrode. For an in-depth investigation of the role of the ZnO EELs, we processed ZnO layers with different morphologies, i.e. closely packed ZnO layers or with nanoscopic holes as shown in **Figure S2**. This could be obtained by processing ZnO EELs using solution of lower ZnO nanoparticle concentration, while keeping identical solvent and deposit conditions. **Figure S2** and **Table S1** depict the time evolution of photovoltaic parameters during a post-annealing treatment at 140°C as a function of the ZnO-based layer morphology. Importantly, we find similar degradation for ZnO EELs containing holes as observed for bare Al contacts (see **Figure 2** and **Table 1**). This clearly indicates that not only the ZnO material itself but also a densely packed layer morphology are crucial to obtain high thermal stability in PSCs (92% of the initial efficiency for a densely packed ZnO EELs after one day vs. 30% for a partially covering ZnO EELs). In the case of a non-annealed solar cell based on a densely packed ZnO EEL, losses of PCE are higher with 84% of the initial efficiency after one day (**Figure S3** and **Table S2**). This drastic initial loss can be addressed to the presence of DIO in the blend.[38] It should be mentioned that we also varied the thickness of the Ca layers from 10 to 30 nm to ensure that the Ca EEL is complete without any pinholes. In all cases, we observed strong degradation under a post-annealing treatment at 140°C demonstrating that not layer porosity is at the origin of the degradation of Ca EELs based solar cells, but the material Ca itself.

As next step, we studied the role of the PEDOT:PSS as HEL in the thermal stability of the studied solar cells. To evaluate the effect of the HEL, we process devices using densely packed ZnO based EELs together with a bare ITO anode. As it can be seen in **Table 1**, the lack of PEDOT:PSS generates solar cells with much lower initial efficiencies of 2.38% as can be expected from literature since PEDOT:PSS improves hole extraction at the anode.[50] But more importantly, thermal stress at 140°C leads to a very fast degradation of all photovoltaic parameters with a loss of more than 60% of the initial PCE only after 1 hour. These results indicate that ITO is by far the most reactive interface of the solar cell and more importantly, PEDOT:PSS is a very efficient material to protect the polymer blend against thermally induced damages from the transparent ITO anode.

PEDOT:PSS and densely packed ZnO nanoparticle based ILs could be identified as highly stable materials protecting polymer solar cells against thermal damage during annealing in a double-sided confinement. However, there is a common feature, a small degradation in performance and more precisely in FF that occurs in all devices during the first few minutes. Indeed, as it can be seen in **Figures 2** and **S2**, in all device configurations identical losses in FF occur within the first 10 min of the post-annealing treatment at 140°C, while further but slower decrease in FF follows depending on the IL material used. There is only one exception, which are solar cells processed without PEDOT:PSS that show constant values of FF during the first 10 min. It seems therefore likely that the initial fast degradation in FF is related to the interface between PEDOT:PSS and the polymer blend. Further studies are however needed to study the origin of the drop in FF in more detail. It leads to a non-negligible average loss of 10% in this parameter and will be addressed in future work.

3.2. Blend composition related thermal degradation in polymer solar cells

From literature it is known that PTB7:$PC_{60}BM$ blends rapidly form large fullerene crystals under thermal stress at 140-150°C,[30,32] while PTB7:$PC_{70}BM$ blends, as shown previously, are

stable at such temperatures.[38] The difference in thermal stability related to the size of the fullerene crystals was attributed to local minima in the mixing enthalpy of the blend, forming only stable phases in the case of PTB7:$PC_{70}BM$.[38] The low thermal stability related to the use of $PC_{60}BM$ was first verified by comparing light microscope images of as-cast PTB7:$PC_{60}BM$ blends with of those exposed to thermal annealing at 140°C during 1 day. As it can be seen in, **Figure S4** the annealed blends clearly show the formation of larger structures, most likely fullerene crystals. Wantz *and coll.* have recently demonstrated that the performances of PTB7:$PC_{60}BM$ solar cells degrade rapidly from 5% to 0.9% after heating for 16 h at 150°C.[32] The strong loss in performance was associated to the thermal instability of the polymer blend. It is important to mention that the authors first annealed the polymer blend at 150°C before completing the device with a successive deposition of Ca and Al. In such a study, only one side of the polymer blend is in contact with an IL during annealing (here the supporting substrate layer) thus leading to a single-sided confinement. The application of thermal annealing to this device stack can be defined as a thermal pre-annealing process. In the present study, we choose to complete first the PTB7:$PC_{60}BM$ based solar cells by spin-coating a densely packed ZnO layer on top of the blend, depositing the Al contact by thermal evaporation and subsequently do the annealing step, here called post-annealing process. Furthermore, we compare the obtained performances to those of solar cells using identical final device structures but exposed to a pre-annealing step at 140°C during 24 h. **Figure 3** provides a schematic representation of both thermal annealing processes, i.e. post-annealing and pre-annealing, together with the corresponding confinement, i.e. double- and single-sided confinements. **Figures 4** and **5** compare the evolution of J-V curves and the photovoltaic parameters of the PTB7:$PC_{60}BM$ solar cells between pre- and a post-annealing treatments as a function of the applied annealing time. **Table S3** summarizes the photovoltaic parameter values.

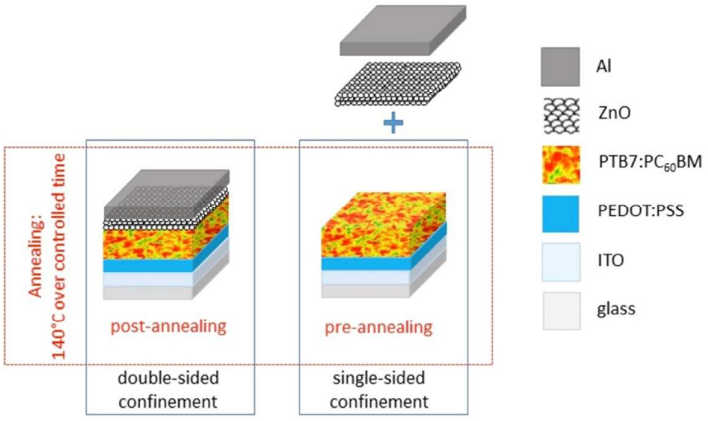

Figure 3. Schematic representation of thermal stress treatments applied to stack layers in double- and single-sided confinements. The thermal annealing at 140°C was either applied directly on the complete PTB7:$PC_{60}BM$ solar cell (post-annealing) or before the ZnO and Al depositions (pre-annealing).

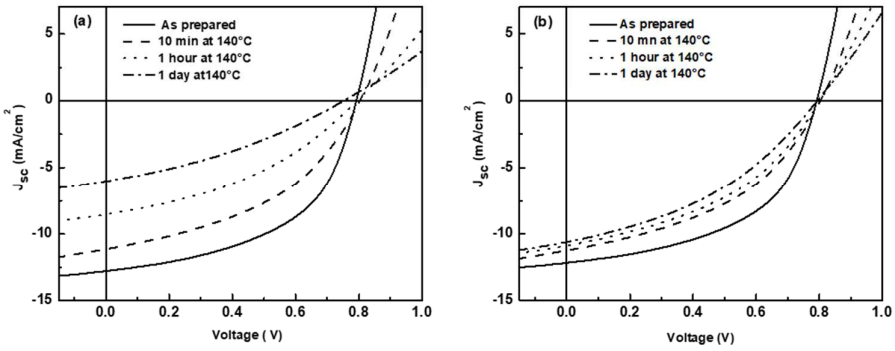

Figure 4. Time evolution of J-V curves of PTB7:$PC_{60}BM$ solar cells as function of (a) pre-annealing (single-sided confinement) and (b) post-annealing (double-sided confinement) thermal stress. The device structure is ITO/PEDOT:PSS/PTB7:$PC_{60}BM$/ZnO/Al.

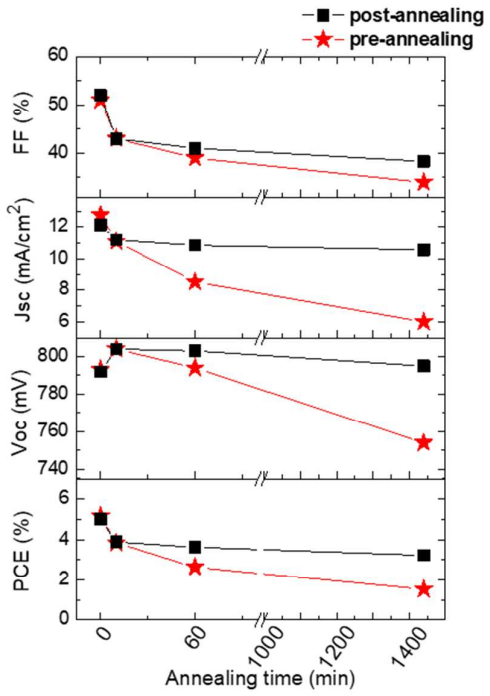

Figure 5. Time evolution of photovoltaic parameters (FF, J_{sc}, V_{oc} and PCE) of PTB7:$PC_{60}BM$ solar cells as function of post-annealing (double-sided confinement) and pre-annealing (single-sided confinement) thermal stress.

As expected for both applied annealing processes, we observe a degradation of the performance of the solar cells based on PTB7:$PC_{60}BM$ blends as a function of thermal ageing. However significant differences can be observed according to the thermal annealing process. For the post-annealing step (double-sided confinement), the first hour induces a loss of 28% in the PCE, whereas during further thermal stress at 140°C up to 24 h the performance remains almost constant. More importantly, the photocurrent losses after 24 h in the double-sided confinement are only 12%. This is in stark contrast to the results reported in the literature.[32] In this sense, we also examined the time evolution versus thermal stress of solar cells produced with a pre-annealing step (single-sided confinement). As it can be seen in **Figures 4a and 5**, we observe indeed the well-known strong degradation in these devices

after thermal stress. After a pre-annealing at 140°C over 24 h, the PTB7:PC_{60}BM based solar cell shows a performance loss of 70%. These results clearly show that there is a pronounced difference in thermally induced degradation as a function of the selected annealing treatment. Moreover, our post-annealing process strongly improves the thermal stability of the solar cells, although the uncovered polymer blend itself rapidly forms fullerene crystals under these conditions (**Figure S4**). As shown in **Figure S5** and **Table S3,** extension of the thermal stress to 3 days only leads to a final loss of 15.5% in photocurrent density highlighting that after an initial 12% drop in photocurrent within the first hour, the photocurrent remains almost stable. Our observation suggests that the nanoscale morphology of unstable PTB7:PC_{60}BM blends is stabilized after the first hour of annealing in a double-sided confinement while no further changes is induced upon prolonged thermal stress treatment.

To understand this stabilization phenomenon, we focus on the role of layer confinement during thermal annealing of the polymer blend. Indeed in the post-annealing step, the PTB7:PC_{60}BM blend is in a double-sided confinement, i.e. sandwiched between PEDOT:PSS and ZnO ILs. Therefore we compared the morphology of bare polymer-fullerene blends processed on PEDOT:PSS (single-sided confinement) to an identical blend layer but covered with a densely packed ZnO layer (double-sided confinement). The latter case allows simulating the situation inside the device stack upon annealing. **Figure 6** shows light microscopic images of PTB7:PC_{60}BM blend layers deposited onto ITO covered with PEDOT:PSS as single- or double-sided confined active layers after a thermal stress at 140°C for 1 day.

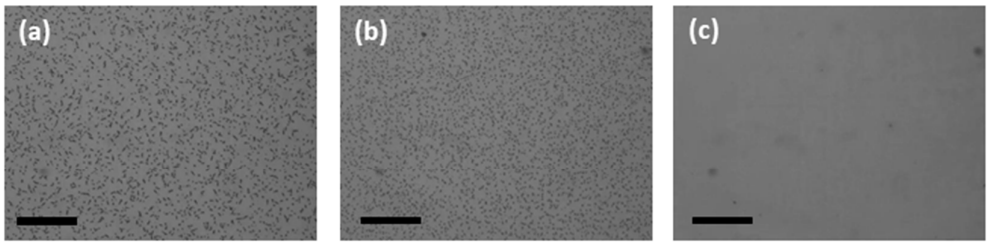

Figure 6. Light microscope images of PTB7:$PC_{60}BM$ blend layers deposited onto ITO covered with PEDOT:PSS and exposed to a thermal stress at 140°C for 1 day in single- (a) and double-sided (b, c) confinement. The thermal annealing at 140°C for 1 day was applied on the bare PTB7:$PC_{60}BM$ layer (a), on the blend layer before the ZnO deposition in (b) or on the ZnO covered PTB7:$PC_{60}BM$ layer in (c). Scale bare corresponds to 100 μm.

In the case of a single-sided PTB7:$PC_{60}BM$ blend layer (**Figure 6a**), black spots can be seen which can be assigned to the well-known fullerene crystals.[38] Hence, this sample can be classified as a thermally unstable polymer-fullerene blend. Almost identical images with expected fullerene crystals are obtained from PTB7:$PC_{60}BM$ blends processed with the pre-annealing step (**Figure 6b**). In contrast, PTB7:$PC_{60}BM$ blend layers covered with ZnO during the thermal annealing do not show fullerene crystals after 24 h at 140°C (**Figure 6c**). Similar results have been observed for PTB7:$PC_{60}BM$ blends deposited directly on bare ITO without PEDOT:PSS as HEL (**Figure S6**) indicating that the stabilization effect is independent of the bottom confinement and only related to the top confinement. These analyses reveal that the presence of a ZnO layer during thermal annealing and successive thermal stress suppresses the formation of $PC_{60}BM$ crystals. A double-sided spatial confinement reduces the mobility of $PC_{60}BM$ molecules and thus its crystallization kinetics in the BHJ layer.[45] The stabilization effect of ZnO is in accordance with the small losses in photocurrent density of only 11% during the post-annealing of the entire solar cells. However, whilst the optical analysis shows the lack of crystal formation, it is possible that there are still morphological changes at the

nanoscale occurring during the annealing of PTB7:$PC_{60}BM$ blends in the double-sided confinement.

3.3 Correlating blend morphology to photocurrent density losses

To investigate potential modification of the nanoscale morphology of the PTB7:$PC_{60}BM$ blend in the two-sided confinement, we applied AFM analysis and electron spectroscopic imaging in transmission electron microscopes either in scanning mode (STEM) or in imaging mode (TEM) (see Experimental Section for details). ESI as imaging technique is based on the recording of spatially resolved spectra of optical excitations that allow to distinguish between donor-enriched and acceptor-enriched phases of the polymer blends.[49,50] Furthermore, mixed phases can be identified.[51] Analyses were conducted on PTB7:$PC_{60}BM$ blends deposited onto PEDOT:PSS which were annealed for 1 day at 140°C either as bare PTB7:$PC_{60}BM$ blends or PTB7:$PC_{60}BM$ blends covered with a densely packed ZnO layer. Performing ESI on bare blend layers allows to directly record signals from the organic materials. By fitting the bulk plasmon peak for each spectrum to a Lorentzian, varying peak energies from the different material phases can be visualized and represented as plasmon peak maps.[49] The resulting map for the bare blend (i.e. single-sided confinement) after thermal annealing at 140°C during 1 day is depicted in **Figure 7a**. As expected the thermally stressed layer shows a very large fullerene aggregate with a size of well over one micrometer. This confirms that in **Figure 6a** and **Figure 6b** the dark spots are fullerene aggregates. More large aggregates as in **Figure 7a** are shown in **Figures S7** and **S8** in dark-field STEM images. **Figure S7** also provides as comparison a dark-field STEM image from a blend layer covered by ZnO. Here, no large fullerene crystals are observed. Together with the light microscopy image in **Figure 6c**, this proves that the ZnO capping layer prevents aggregate formation.

Except for the large $PC_{60}BM$ aggregate, changes in the nanoscale morphology is of high importance. The as-cast PTB7:$PC_{60}BM$ blend depicted in **Figure S9** shows an optimized BHJ

of donor and acceptor enriched phases separated by tens of nanometers, while a large amount of mixed phase is present. From **Figure 7a** it can be deduced that the size of the material-enriched domains and their distance to each other increase upon thermal stress, whilst the amount of mixed phases is strongly reduced. In **Figure 7b** the plasmon peak map of the annealed layer with ZnO capping is presented still revealing the morphology of the organic blend. However, the ZnO layer contributes to the recorded spectra from the ESI-TEM data so that a detailed comparison to the non-capped layer would not be possible. To quantify ZnO contributions in the spectroscopic data, the low-energy-loss spectrum of pure ZnO was taken from a previous 3D analysis of a tandem cell,[49] and used together with spectra from pure PTB7 and $PC_{60}BM$ for a least-squares fitting of the experimental spectra. Since in total the films were thinner than the inelastic mean-free-path of the high-energy electrons, the fraction of the ZnO signal could be determined and subtracted from the spectra to reconstruct the PTB7:$PC_{60}BM$ signals. Subsequently, the energies of the plasmon peak positions were again determined as before for the bare layer by fitting the spectra to a Lorentzian model. Typically, this correction leads to slightly elevated plasmon peak energies in the map. To the best of our knowledge this is the first time that such morphological analyses at the nanoscale are performed across a ZnO capping layer. More details on the analysis are given in the Experimental Section and in the supporting information (**Figure S10** and **Figure S11**). The resulting plasmon peak map from the blend with ZnO capping, reconstructed to represent only PTB7:$PC_{60}BM$ signals, is shown in **Figure 7c**. Interestingly, except for the lack of large $PC_{60}BM$ clusters, the general nanoscale morphology of this blend features similar sizes and distances between donor and acceptor enriched domains as the comparable blend annealed without ZnO capping layer. This is confirmed by providing plasmon peaks maps in **Figure 8** from different regions on the samples and in higher magnification. For the uncovered layer (**Figure 8a**) a region further away from a fullerene cluster was selected to ensure that the domain compositions were not altered locally due to aggregation of fullerene molecules.

These results imply that during thermal annealing of PTB7:$PC_{60}BM$ blends the ZnO capping layer particularly inhibits only the formation of large, micrometre-sized fullerene crystals at the surface of the blend layer, whereas morphological changes inside the blend related to an enlargement of the domain size and distances between enriched-donor and enriched-acceptor domains occur in both cases. In particular the average distance between donor and acceptor enriched domains increases from 10 to 50 nm (manual centre-to-centre distance measurements from enriched domains) together with a reduced amount of the mixed phase (yellow phases in the STEM-SI images) during the thermal annealing (see **Figure S9** to compare).

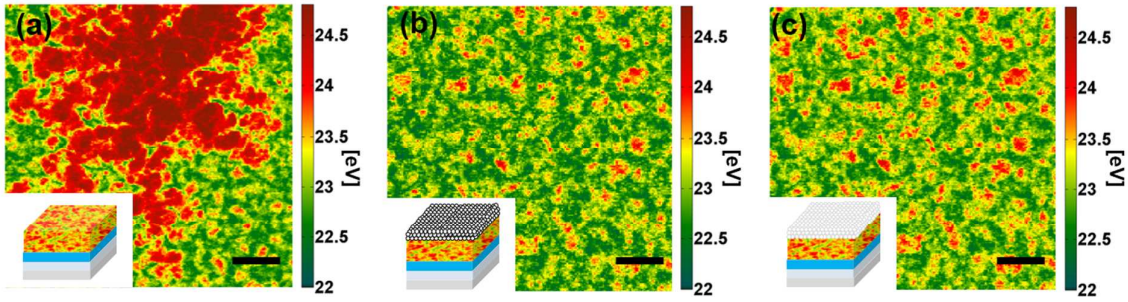

Figure 7. Plasmon peak maps of uncovered (single-sided confinement; a) and ZnO covered (double-sided confinement; b, c) PTB7:$PC_{60}BM$ blends after thermal annealing at 140°C during 1 day showing the nanoscale materials phases ($PC_{60}BM$ rich domains in red with high plasmon peak energy and PTB7 rich domains in green with low energy). As seen in (a), large $PC_{60}BM$ aggregates appear only for thermally stressed single-sided confined layers. For (c) the spectral contribution of the ZnO capping layer was removed from the data so that plasmon peak energies can be compared to the map in (a). Scale bars represent 200 nm.

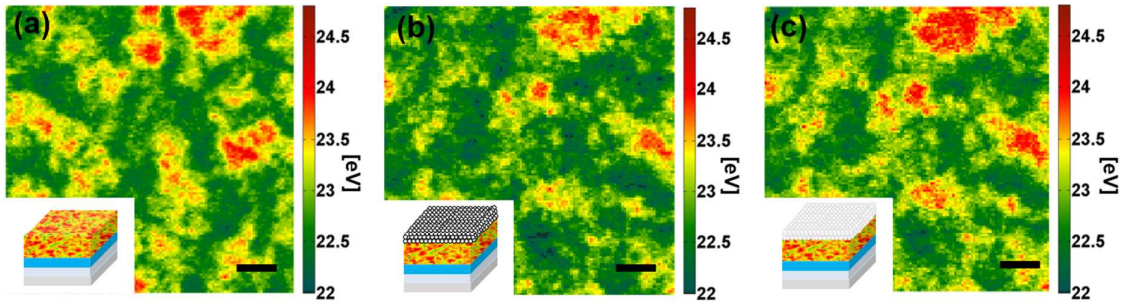

Figure 8. Higher magnification plasmon peak maps of uncovered (single-sided confinement; a) and ZnO covered (double-sided confinement; b, c) PTB7:$PC_{60}BM$ blends after thermal annealing at 140°C during 1 day showing the nanoscale materials phases. For (c) the spectral contribution of the ZnO capping layer was removed from the data so that plasmon peak energies can be compared to the map in (a). The structure of layers at smaller length scales (in comparison to **Figure 7**) is independent of confinement. Scale bars represent 50 nm.

In the following we correlate the changes in the photovoltaic parameters observed during the thermal annealing by using either single-sided or double-sided confinement with the ongoing changes in the blend morphology. Taking into account that in both cases an enlargement of the domain size and spacing occur during thermal annealing at 140°C, we would expect that photocurrent density is strongly reduced also in the case of double-sided confinement, i.e. ZnO capped blend layers, due to the excitonic nature of the material. However, the photocurrent density is only reduced by 12% with a maximal J_{SC} of 12.15 mA/cm^2 for the as-cast solar cell and 10.59 mA/cm^2 after a post-annealing at 140°C for 1 day (see **Table S3**). Thus the increase in domain size during thermal annealing appears to be in stark contrast to the small drop in photocurrent. This result suggests that in the thermally altered blends there is still be efficient exciton dissociation followed by charge carrier collection. To understand this phenomenon, the evolution of FF during annealing provides important indications. It can be seen in **Table S3** that while J_{SC} is almost not affected, FF is strongly reduced from 52% to 38.3% after 1 day of post-annealing. The latter points to strongly elevated charge carrier

recombination inside the thermally modified blend, which can be correlated to the enlargement of domain spacing. Taking these results into account we suggest that the high J_{SC} in post-annealed (double-sided confined) solar cells can be explained by sufficiently high electron transport via hopping inside the donor enriched domains allowing the extraction of theses electrons towards the fullerene enriched domains under short circuit conditions and thus maximal internal field. C.H.Y. Ho *et al.* have shown very recently that fullerene percolation occurs already at low PTB7:fullerene ratio of 1:0.1 leading to reduction in fullerene trap density and increase in electron mobility by several orders of magnitude.[53]

To evaluate the presence of fullerene inside the donor enriched phase, the spatially resolved plasmon peak energies of **Figure 7** and **Figure 8** can be compared to pure materials reference spectra. **Figure S11** shows the recorded spectrum of pure PTB7 indicating that a plasmon peak energy of ca. 21.7 eV for the pure donor and contrasts with the peak energies shown e.g. in **Figure 7** and **Figure 8** are in general higher inside the PTB7 enriched phase. This implies a non-negligible fullerene concentration inside the donor enriched phase and thus the possibility to enable fullerene percolation inside the PTB7:$PC_{60}BM$ blend. In order to study more in detail the photocurrent generation inside the polymer blend before and after annealing, external quantum efficiency measurements were used. As it can be seen in **Figure S12**, an almost constant loss in photocurrent generation over the whole absorption spectrum accompanies the morphological changes during annealing. Taking into account that the $PC_{60}BM$ contributes to the photocurrent generation through light absorption in the range of 340 to 500 nm and PTB7 dominates absorption from 450 to 780 nm, it can thus be considered that the thermal annealing and thus the on-going morphological changes impact only weakly the photocurrent generation inside the donor and acceptor phases. Therefore, the high photocurrent observed under J_{SC} conditions indicates that hole and electron transports occur not only in the mixed phase but that minority charge carrier transport continues also inside the enriched phases, i.e. holes inside the acceptor enriched phase and electrons inside the donor

enriched phase. This allows transporting these minority charge carriers towards to their corresponding enriched domains followed by charge extraction towards the electrode under the high internal field.

5. Conclusion

Understanding and reducing thermal degradation of polymer solar cells is highly essential for the introduction of this technology into application. In this work, we first identify the thermal stability of polymer solar cells as a function of cathode buffer layer used. Here, densely packed ZnO nanoparticle layers are found to be particularly suitable to gain high temperature stability at thermal stress at 140°C. In the second part, application of thermally stable ILs, i.e. densely packed ZnO EELs in combination with PEDOT:PSS as HELs, was used to study in how far ZnO EELs that are simultaneous a capping layer for surface of the blend can affect the degradation of a solar cell under thermal stress using a thermally unstable polymer blend. We demonstrate that the improved thermal stability in double-sided confinement could be addressed to the beneficial effect of a double-sided confinement during the thermal annealing process compared to annealing of an uncovered single-sided blend. The ZnO capping EELs particularly inhibit the formation of micrometre-sized fullerene crystals at the surface of the blend layer and leads to a stabilization of the nanoscale morphology of a thermally unstable blend such as PTB7:$PC_{60}BM$ by increasing only the domain spacing by a factor of 5. The comparably small photocurrent density losses in the stabilized blend points towards the existence of efficient ambipolar transport inside donor and acceptor enriched phases in PTB7:$PC_{60}BM$ blends. Our results thus open new insights in thermal stabilization of solar cells using ILs and designing novel polymer blends with improved tolerance against thermally induced nanoscale changes in morphology.

Acknowledgements

We acknowledge financial support by the French *Fond Unique Interministériel* (FUI) under the project "SFUMATO" (Grant number: F1110019V/201308815) as well as by the European Commission under the Project "SUNFLOWER" (FP7-ICT-2011-7-contract number: 287594). MP and RRS acknowledge support by the HeiKA (Heidelberg Karlsruhe Research Partnership) FunTech-3D materials science program.

Supporting Information. Additional time evolution of J-V curves and photovoltaic parameters of PTB7:$PC_{70}BM$ and PTB7:$PC_{60}BM$ solar cells. Light microscope images of as-cast and thermally stressed PTB7:$PC_{60}BM$ blends. Light microscope images of PTB7:$PC_{60}BM$ blend layers. Dark-field STEM images of PTB7:$PC_{60}BM$ blend layers. Plasmon peak maps of as-cast and ZnO covered PTB7:$PC_{60}BM$ blends. Contribution of ZnO to dark-field TEM and energy-loss signals. Electron energy-loss spectrum of pure PTB7 layer. EQE spectra of PTB7:$PC_{60}BM$ solar cell.

AUTHOR INFORMATION

Corresponding Authors

* *E-mail address*: videlot@cinam.univ-mrs.fr (C. Videlot-Ackermann) *and* ackermann@cinam.univ-mrs.fr (J. Ackermann)

Author Contributions

The manuscript was written through contributions of all authors. All authors have given approval to the final version of the manuscript.

References

(1) You J.; Dou L.; Yoshimura K.; Kato T.; Ohya K.; Moriarty T.; Emery K.; Chen C.-C.; Gao J.; Li G.; Yang Y. A Polymer Tandem Solar Cell with 10.6% Power Conversion Efficiency. *Nat. Commun*. **2013**, 4, 1446.

(2) Li W.; Hendriks K.H.; Roelofs W.S.C.; Kim Y.; Wienk M.M.; Janssen R.A.J. Efficient Small Bandgap Polymer Solar Cells with High Fill Factors for 300 nm Thick Films. *Adv. Mater.* **2013**, 25, 3182-3186.

(3) Li Y. Molecular Design of Photovoltaic Materials for Polymer Solar Cells: Toward Suitable Electronic Energy Levels and Broad Absorption. *Acc. Chem. Res.* **2012**, 45, 723-733.

(4) Li N.; Brabec C.J. Air-processed polymer tandem solar cells with power conversion efficiency exceeding 10%. *Energy Environ. Sci.* **2015**, 8, 2902-2909.

(5) Ben Dkhil S.; Pfannmöller M.; Bals S.; Koganezawa T.; Yoshimoto N.; Hannani D.; Gaceur M.; Videlot-Ackermann C.; Margeat O.; Ackermann J. Square-Centimeter-Sized High-Efficiency Polymer Solar Cells: How the Processing Atmosphere and Film Quality Influence Performance at Large Scale. *Adv. Energy Mater.* **2016**, 6, 1600290.

(6) Zuo L.; Zhang S.; Li H.; Chen H. Toward Highly Efficient Large-Area ITO-Free Organic Solar Cells with a Conductance-Gradient Transparent Electrode. *Adv. Mater.* **2015**, 27, 6983-6989.

(7) Hong S.; Kang H.; Kim G.; Lee S.; Kim S.; Lee J.-H.; Lee J.; Yi M.; Kim J.; Back H.; Kim J.-R.; Lee K. A Series Connection Architecture for Large-Area Organic Photovoltaic Modules with a 7.5% Module Efficiency. *Nat. Commun*. **2016**, 7, 10279.

(8) Zhao W.; Li S.; Yao H.; Zhang S.; Zhang Y.; Yang B.; Hou J. Molecular Optimization Enables over 13% Efficiency in Organic Solar Cells. *J. Am. Chem. Soc.* 2017, 139, 7148-7151.

(9) Jørgensen M.; Norrman K.; Gevorgyan S.-A.; Tromholt T.; Andreasen B.; Krebs F.C. Stability of Polymer Solar Cells. *Adv. Mater.* **2012**, 24, 580-612.

(10) Habisreutinger S.N.; McMeekin D.P.; Snaith H.J.; Nicholas R.J. Research Update: Strategies for improving the stability of perovskite solar cells. *APL Materials* **2016**, 4, 091503.

(11) Zhao X.; Kim H.-S.; Seo J.-Y.; Park N.-G. Effect of Selective Contacts on the Thermal Stability of Perovskite Solar Cells. *ACS Appl. Mater. Interfaces* **2017**, 9, 7148-7153.

(12) Asghar M.I.; Zhang J.; Wang H.; Lund P.D. Device Stability of Perovskite Solar Cells – A Review. *Renewable and Sustainable Energy Reviews* 2017, 77, 131-146.

(13) Niu G.; Li W.; Li J.; Liang X.; Wang L. Enhancement of Thermal Stability for Perovskite Solar Cells Through Cesium Doping. *RSC Adv*. **2017**, 7, 17473-17479.

(14) Grossiord N.; Kroon J.M.; Andriessen R.; Blom P.W.M. Degradation Mechanisms in Organic Photovoltaic Devices. *Org. Electron.* **2012**, 13, 432-456.

(15) Cheng P.; Zhan X., Stability of organic solar cells: challenges and strategies. *Chem Soc Rev*. **2016**, 45, 2544-2582.

(16) Gevorgyan S.A.; Madsen M.V.; Roth B.; Corazza M.; Hösel M.; Søndergaard R.R.; Jørgensen M.; Krebs F.C. Lifetime of Organic Photovoltaics: Status and Predictions. *Adv. Energy Mater.* **2016**, 6, 1501208.

(17) Roesch R.; Faber T.; von Hauff E.; Brown T.M.; Lira-Cantu M.; Hoppe H. Procedures and Practices for Evaluating Thin-Film Solar Cell Stability. *Adv. Energy Mater.* **2015**, 5, 1501407.

(18) Yang X.; Loos J.; Veenstra S.C.; Verhees W.H.J.; Wienk M.M.; Kroon J.M.; Michels M.A.J.; Janssen R.A.J. Nanoscale Morphology of High-Performance Polymer Solar Cells. *Nano Lett.* **2005**, 5, 579-583.

(19) Bertho S.; Janssen G.; Cleij T.J.; Conings B.; Moons W.; Gadisa A.; D'Haen J.; Goovaerts E.; Lutsen L.; Manca J.; Vanderzande D. Effect of Temperature on the Morphology and Photovoltaic Stability of Bulk heterojunction polymer:fullerene Solar Cells. *Sol. Energy Mater. Sol. Cells* **2008**, 92, 753-760.

(20) Sivula K.; Ball Z.T.; Watanabe N.; Fréchet J.M.J. Amphiphilic Diblock Copolymer Compatibilizers and Their Effect on the Morphology and Performance of Polythiophene:Fullerene Solar Cells. *Adv. Mater.* **2006**, 18, 206-210.

(21) Renaud C.; Mougnier S.J.; Pavlopoulou E.; Brochon C.; Fleury G.; Deribew D.; Portale G.; Cloutet E.; Chambon S.; Vignau L.; Hadziioannou G. Block Copolymer as a Nanostructuring Agent for High-Efficiency and Annealing-Free Bulk Heterojunction Organic Solar Cells. *Adv Mater.* **2012**, 24, 2196-2201.

(22) Mulherin R.C.; Jung S.; Huettner S.; Johnson K.; Kohn P.; Sommer M.; Allard S.; Scherf U.; Grennham N.C. Ternary Photovoltaic Blends Incorporating an All-Conjugated Donor–Acceptor Diblock Copolymer. *Nano Lett.* **2011**, 11, 4846-4851.

(23) Zhang Y.; Yip H.; Acton O.; Hau S.K.; Huang F.; Jen A.K.Y. A Simple and Effective Way of Achieving Highly Efficient and Thermally Stable Bulk-Heterojunction Polymer Solar Cells Using Amorphous Fullerene Derivatives as Electron Acceptor. *Chem. Mater.* **2009**, 21, 2598-2600.

(24) Meng X.; Zhang W.; Tan Z.; Li Y.; Ma Y.; Wang T.; Jiang L.; Shu C.; Wang C. Highly Efficient and Thermally Stable Polymer Solar Cells with Dihydronaphthyl-Based [70]Fullerene Bisadduct Derivative as the Acceptor. *Adv. Funct. Mater.* **2012**, 22, 2187-2193.

(25) Lin Y.; Lim J.A.; Wie Q.; Mannsfeld S.C.B.; Briseno A.L.; Watkins J.J. Cooperative Assembly of Hydrogen-Bonded Diblock Copolythiophene/Fullerene Blends for Photovoltaic Devices with Well-Defined Morphologies and Enhanced Stability. *Chem. Mater.* **2012**, 24, 622-632.

(26) Liao M.-H.; Tsai C.-E.; Lai Y.-Y.; Cao F.-Y.; Wu J.-S.; Wan C.-L.; Hsu C.-S.; Liau I.; Cheng Y.-J. Morphological Stabilization by Supramolecular Perfluorophenyl-C_{60} Interactions Leading to Efficient and Thermally Stable Organic Photovoltaics. *Adv. Funct. Mater*. **2014**, 24, 1418-1429.

(27) Bertho S.; Campo B.; Piersimoni F.; Spoltore D.; D'Haen J.; Lutsen L.; Maes W.; Vanderzande D.; Manca J. Improved Thermal Stability of Bulk Heterojunctions Based on Side-Chain Ffunctionalized Poly(3-alkylthiophene) Copolymers and PCBM. *Sol. Energy Mater. Sol. Cells* **2013**, 110, 69-76.

(28) Gevorgyan S.A.; Krebs F.C. Bulk Heterojunctions Based on Native Polythiophene. *Chem. Mater*. **2008**, 20, 4386-4390.

(29) Li Z.; Wong H.C.; Huang Z.; Zhong H.; Tan C.H.; Tsoi W.C.; Kim J. S.; Durrant J. R.; Cabral J.T. Performance Enhancement of Fullerene-Based Solar Cells by Light Processing. *Nat. Commun*. **2013**, 4, 2227.

(30) Wong H.C.; Li Z.; Tan C.H.; Zhong H.; Huang Z.; Bronstein H.; McCulloch I.; Cabral J.T.; Durrant J.R. Morphological Stability and Performance of Polymer–Fullerene Solar Cells under Thermal Stress: The Impact of Photoinduced $PC_{60}BM$ Oligomerization. *ACS Nano* **2014**, 2, 1297-1308.

(31) Wantz G.; Derue L .; Dautel O.; Rivaton A.; Hudhommed P.; Dagron-Lartigaue C. Stabilizing Polymer-Based Bulk Heterojunction Solar Cells via Crosslinking. *Polym. Int.* **2014**, 63, 1346-1361.

(32) Derue L.; Dautel O.; Tournebize A.; Drees M.; Pan H.; Berthumeyrie S.; Pavageau B.; Cloutet E.; Chambon S.; Hirsch L.; Rivaton A.; Hudhomme P.; Facchetti A.; Wantz G. Thermal Stabilisation of Polymer–Fullerene Bulk Heterojunction Morphology for Efficient Photovoltaic Solar Cells. *Adv. Mater.* **2014**, 26, 5831-5838.

(33) Lindqvist C.; Bergqvist J.; Bäcke O.; Gustafsson S.; Wang E.; Olsson E.; Inganäs O.; Andersson M.R.; Müller C. Fullerene Mixtures Enhance the Thermal Stability of a Non-Crystalline Polymer Solar Cell Blend. *Appl. Phys. Lett*. **2014**, 104, 153301.

(34) Lindqvist C.; Sanz-Velasco A.; Wang E.; Backe O.; Gustafsson S.; Olsson E.; Andersson M.R.; Müller C. Nucleation-Limited Fullerene Crystallisation in a Polymer–Fullerene Bulk-Heterojunction Blend. *J. Mater. Chem. A* **2013**, 1, 7174-7180.

(35) Diaz de Zerio Mendaza A.; Bergqvist J.; Bäcke O.; Lindqvist C.; Kroon R.; Gao F.; Andersson M.R.; Olsson E.; Inganäs O.; Müller C. Neat C_{60}:C_{70} Buckminsterfullerene Mixtures Enhance Polymer Solar Cell Performance. *J. Mater. Chem. A* **2014**, 2, 14354-14359.

(36) Lindqvist C.; Bergqvist J.; Feng C.-C.; Gustafsson S.; Bäcke O.; Treat N.D.; Bounioux C.; Henriksson P.; Kroon R.; Wang E.; Sanz-Velasco A.; Kristiansen P.M.; Stingelin N.; Olsson E.; Inganäs O.; Andersson M.R.; Müller C. Fullerene Nucleating Agents: A Route Towards Thermally Stable Photovoltaic Blends. *Adv. Energy. Mater*. **2014**, 4, 1301437.

(37) Richards J.J.; Rice A.H.; Nelson R.D.; Kim F.S.; Jenekhe S.A.; Luscombe C.K.; Pozzo D.C. Modification of PCBM Crystallization via Incorporation of C_{60} in Polymer/Fullerene Solar Cells. *Adv. Funct. Mater.* **2013**; 23, 514-521.

(38) Ben Dkhil S.; Pfannmöller M.; Saba M.I.; Gaceur M.; Heidari H.; Videlot-Ackermann C.; Margeat O.; Guerrero A.; Bisquert J.; Garcia-Belmonte G.; Mattoni A.; Bals S.; Ackermann J. Toward High-Temperature Stability of PTB7-Based Bulk Heterojunction Solar Cells: Impact of Fullerene Size and Solvent Additive. *Adv Energy Mater.* **2017**, 7, 1601486.

(39) Hains A.W.; Liu J.; Martinson A. B. F.; Irwin M. D.; Marks T. J. Anode Interfacial Tuning via Electron-Blocking/Hole-Transport Layers and Indium Tin Oxide Surface Treatment in Bulk-Heterojunction Organic Photovoltaic Cells. *Adv. Funct. Mater.* **2010**, 20, 595-606.

(40) Son H.J.; Kim S.H.; Kim D.H. Critical Impact of Hole Transporting Layers and Back Electrode on the Stability of Flexible Organic photovoltaic Module. *Adv. Energy Mater*. **2016**, 7, 1601289.

(41) Lee S. T.; Gao Z. Q.; Hung L. S. Metal Diffusion from Electrodes in Organic Light-Emitting Diodes. *Appl. Phys. Lett.* **1999**, 75, 1404.

(42) Suemori K.; Yokoyama M.; Hiramoto M. Electrical Shorting of Organic Photovoltaic Films Resulting from Metal Migration. *J. Appl. Phys*. **2006**, 99, 036109.

(43) Uhrich C.; Schueppel R.; Petrich A.; Pfeiffer M.; Leo K.; Brier E.; Kilickiran P.; Baeuerle P. Organic Thin-Film Photovoltaic Cells Based on Oligothiophenes with Reduced Bandgap. *Adv. Funct. Mater*. **2007**, 17, 2991-2999.

(44) Kumar A.; Sista S.; Yang Y. Dipole Induced Anomalous S-Shape *I-V* Curves in Polymer Solar Cells. *J. Appl. Phys*. **2009**, 105, 094512.

(45) Yang X.; Alexeev A.; Michels M.A.J.; Loos J. Effect of Spatial Confinement on the Morphology Evolution of Thin Poly(*p*-phenylenevinylene)/Methanofullerene Composite Films. *Macromolecules* **2005**, 38, 4289-4295.

(46) Wang T.; Chen C.; Guo K.; Chen G.; Xu T.; Wei B. Improved Performances of Polymer Solar Cells by Using Inorganic, Organic, and Doped Cathode Buffer Layers. *Chin. Phys. B* **2016**, 25, 038402.

(47) Ben Dkhil S.; Duché D.; Gaceur M.; Thakur A.K.; Bencheikh Aboura F.; Escoubas L.; Simon J.-J.; Guerrero A.; Bisquert J.; Garcia-Belmonte G.; Bao Q.; Fahlman M.; Videlot-Ackermann C.; Margeat O.; Ackermann J. Interplay of Optical, Morphological and Electronic Effects of ZnO Optical Spacers in Highly Efficient Polymer Solar Cells. *Adv. Energy Mater.* **2014**, 4, 1400805.

(48) Mattioli G.; Ben Dkhil S.; Saba M.I.; Malloci G.; Melis C.; Alippi P.; Filippone F.; Giannozzi P.; Thakur A.K.; Gaceur M.; Margeat O.; Diallo A.K.; Videlot-Ackermann C.; Ackermann J.; Bonapasta A.A.; Mattoni A. Interfacial Engineering of P3HT/ZnO Hybrid Solar Cells Using Phthalocyanines: A Joint Theoretical and Experimental Investigation. *Adv. Energy Mater.* **2014**, 4, 1301694.

(49) Pfannmöller M.; Heidari H.; Nanson L.; Lozman O. R.; Chrapa M.; Offermans T.; Nisato G.; Bals S. Quantitative Tomography of Organic Photovoltaic Blends at the Nanoscale. *Nano Lett*. **2015**, 15, 6634-6642.

(50) Guerrero A.; Pfannmöller M.; Kovalenko A.; Ripolles T.S.; Heidari H.; Bals S.; Kaufmann L.-D.; Bisquert J.; Garcia-Belmonte G. Nanoscale Mapping by Electron Energy-Loss Spectroscopy Reveals Evolution of Organic Solar Cell Contact Selectivity. *Org. Electron*. **2015**, 16, 227-233.

(51) Pfannmöller M.; Flügge H.; Benner G.; Wacker I.; Sommer C.; Hanselmann M.; Schmale S.; Schmidt H.; Hamprecht F.A.; Rabe T.; Kowalsky W.; Schröder R.R. Visualizing a Homogeneous Blend in Bulk Heterojunction Polymer Solar Cells by Analytical Electron Microscopy. *Nano. Lett.* **2011**, 11, 3099-3107.

(52) Lai T.-H.; Tsang S.-W.; Manders J.R.; Chen S.; So F. Properties of interlayer for organic photovoltaics. *Mater. Today* **2013**, 16, 424-432.

(53) Ho C. H. Y.; Cheung S-H.; Li H.W.; Chiu K. L.; Cheng Y.; Yin H.; Chan M.H.; So F.; Tsang S.W.; So S.K. Using Ultralow Dosages of Electron Acceptor to Reveal the Early Stage Donor–Acceptor Electronic Interactions in Bulk Heterojunction Blends. *Adv. Energy Mater.* **2017**, 7, 1602360.

Graphical abstract

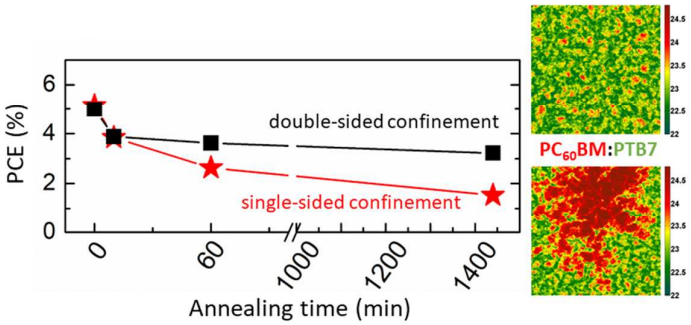

Highlights

- Study of thermal degradation in polymer solar cells based on PTB7 and fullerene derivatives
- Stable EELs and double-sided confinement within the device for high thermal stability
- Study of the nanoscale morphology of the blends in the two-sided confinement
- Suppression of extensive fullerene diffusion by the double-sided confinement